Spectral Index for classifying glacier debris distribution and thickness using Multispectral UAV imagery: A case study at Juncal Norte Glacier, Central Andes of Chile.

Luis Muñoz[1,2], Carlos Cárdenas[1], Javier L. Armijo Quiñones[2], Natalia Mestre[2], Erling Johnson[1], Francisco Fernandoy[2]

[1] Universidad de Magallanes, UMAG, Chile - luismugaet@gmail.com, carlos.cardenas@umag.cl, erling.johnson@umag.cl
[2] Laboratorio de Análisis Isotópicos, Universidad Andrés Bello, Chile - luismugaet@gmail.com, arqui.geologia@gmail.com, nmestresilva@gmail.com, francisco.fernandoy@unab.cl

Keywords: Chilean Andes Cordillera, Debris cover glacier, Multispectral image, UAV, spectral index.

Abstract

Understanding of debris-covered glaciers is crucial for predicting melt dynamics in high-mountain regions. Juncal Norte Glacier, located on the northwestern slope of Nevado Juncal in central Chile, has experienced a marked retreat—losing 22% of its surface area between 1955 and 2022. As it recedes, its lower tongue has become increasingly covered by supraglacial debris, a process that appears to have accelerated in recent years. This study proposes a spectral index (SI) derived from UAV-based multispectral imagery to classify debris thickness and its spatial distribution at Juncal Norte Glacier tongue. Data was collected during three UAV flights in February 2025 using high-resolution sensors. The classification relies on the green, red, red edge, and near-infrared (NIR) bands, enabling detailed surface mapping of the glacier's ablation zone, with a spatial resolution of 11 cm/pixel. Preliminary results indicate that the method captures fine-scale debris heterogeneity and identifies zones of bare ice and varying debris thickness. Future work will focus on refining the spectral approach and integrating the results into geodetic mass balance estimates to improve glacier change assessments.

1. Introduction

Debris-covered glaciers are present in many mountain ranges around the world, including the Chilean Andes, so there is a growing need to understand how they influence the glacier dynamics in order to improve, for example, water resource management. Debris-covered glaciers are progressively gaining importance and visibility as mountain glaciers retreat and become covered with debris (Nicholson and Benn, 2013), becoming an increasingly visible and characteristic feature in central Chile (Pellicciotti et al., 2013). Globally, 44% of mountain glaciers have a sediment cover greater than 0.1 km^2, 15% have a cover greater than 1 km^2, and 20% have substantial cover, exceeding 10 km^2 or 7% of their surface area, which means that 14% of the surface of mountain glaciers is covered with sediments (Herreid and Pellicciotti, 2020). In central Chile, it is estimated that up to a third of the glaciers have substantial debris cover (Pellicciotti et al., 2013).

The supraglacial debris cover on glaciers influences the ablation regime of the underlying ice, altering the surface energy balance and imposing a barrier between the atmosphere and the ice (Nicholson and Benn, 2013). Therefore, the supraglacial debris cover plays a fundamental role in the albedo, which is the proportion of shortwave solar radiation that is reflected from the glacier surface versus the incident radiation. In the case of a thin layer of debris on the glacier surface, the albedo over the debris is lower; therefore, the absorbed thermal energy is efficiently transmitted to the ice, increasing melting compared to bare ice (Nicholson and Benn, 2013). However, as the thickness of the debris cover increases, the thermal energy stored in the debris is retained during the day and returned to the atmosphere at night, therefore in this condition, the melting is lower compared to bare surface ice.

The introduction of remote sensing techniques and the use of satellite data have made it possible to build large global models, which approximately show the total area of covered glaciers (Rounce et al., 2021; Herreid and Pellicciotti, 2020), with the limitation that both the thickness and the composition and extent of the sediment have a strong spatial variation. In this context, the recent introduction of cameras and lightweight sensors mounted on UAVs has made it possible to monitor large areas of ice with a high degree of detail (Fyffe et al., 2020), where the processing of the obtained information allows the classification of glacier surfaces covered with debris at high resolution.

As mountain glaciers retreat and lose mass, they begin a transition from a bare or white glacier, where debris cover increases, to a debris covered glacier, eventually becoming a rock glacier (Jones et al., 2019). Although this is not the only process by which rock glaciers can be generated (Monnier and Kinnard, 2015), it represents a good continuum according to which most debris covered glaciers evolve (Anderson et al., 2018).

The introduction of new forms of UAV monitoring allows the recognition of surface processes that influence ablation, such as ice cliffs and supraglacial lagoons, which act as focal points for ablation on debris covered glaciers and whose dynamics determine the total mass balance of the covered glacier (Sato et al., 2021). Sediment cover is especially important because, as indicated above, thin layers of sediment can reduce glacier albedo, increase the absorption of shortwave radiation, and increase ablation. As sediment accumulates and the cover thickens, it begins to insulate the ice, reducing ablation (Östrem, 1959). The point at which the ice begins to insulate the ice and reduce its ablation is called the critical thickness, and the relationship between sediment thickness and ablation beneath it is called the Östrem curve (Fyffe et al., 2020).

In addition to the thickness of the sediment layer, the Östrem curve is affected by the type of debris (lithology), its size, shape, sediment distribution, the degree of interstitial moisture, among other detrital properties (Nicholson and Benn, 2013; Lukas et al., 2013). Furthermore, sediment cover tends to present significant spatial variability (Rounce et al., 2021). All

This contribution has been peer-reviewed. The double-blind peer-review was conducted on the basis of the full paper.
https://doi.org/10.5194/isprs-annals-X-3-W4-2025-263-2026

of this makes ablation under debris difficult to model, and many of the global models that attempt to predict the behavior of glacial masses do not consider the debris covered areas (Herreid and Pellicciotti, 2020). Since local debris thicknesses are generally unknown and not considered in the models, it is estimated that local ablation could be underestimated by up to 0.4 meters of water equivalent per year (Rounce et al., 2021). Although there are great efforts to close this margin and improve models of debris covered glaciers with real data (Huo et al., 2021; Falaschi et al., 2021; Monnier and Kinnard, 2015), there is still a notable lack of ground observations in South America, especially in central Chile.

Multispectral analysis in glaciology has traditionally been carried out at large scales using satellite data (Racoviteanu et al., 2008). More recently, Jawak et al. (2022) successfully used WorldView multispectral imagery for debris characterization in Himalayan glaciers. Several spectral indices have been developed for detecting snow, ice, and lake ice; among the most widely used are the Normalized Difference Snow Index (NDSI) and the Mid-Infrared Sea and Lake Ice Index (MISI). These indices exploit the high reflectivity of snow and ice in the visible (VIS) and near-infrared (NIR) wavelengths, as well as their relatively high absorption in the mid-infrared spectrum (Dorofy et al., 2016).

Despite this progress, very few studies have applied multispectral analysis using UAV platforms. This is mainly because multispectral UAV systems are not yet widely available and remain expensive. Moreover, most commercial and more affordable UAVs are not equipped with high-quality infrared sensors, making it necessary to develop new indices or classification methods capable of distinguishing between ice and debris-covered ice.

Recent UAV-based studies have primarily focused on mass balance monitoring and debris evolution (Jones et al., 2019; van Woerkom et al., 2019), with particular attention to areas of thick debris cover and clast movement. However, there is still a significant gap in research addressing the transition zones and their effects on glacier mass balance.

The study of the thickness of the supraglacial debris layer becomes relevant for understanding the dynamics of the Juncal Norte glacier, which is located in the Valparaíso region within the Central Andes, flows north along the slope of the Juncal snow-capped mountain, forming a narrow tongue one km wide and approximately 5 km long (Ayala et al., 2017), This tongue is partly composed of debris covered ice, which were fed by the lateral moraines and volcanic rock walls (DGA, 2022a).

2. Study Area

The study area is at the ablation tongue of "Juncal Norte" Glacier (JNG), located on the northwestern slope of Nevado Juncal. It constitutes one of the largest glaciers at the central Chilean Andes cordillera, located 70 kilometres at northeast of Santiago, as can be seen in figure 1A and B.

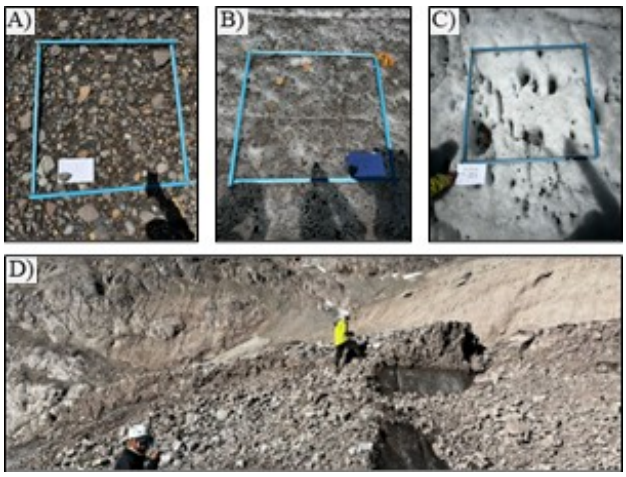

Figure 2: Sampling places. A) Cover glacier, B) Transition zone, C) Exposed Ice, D) Thick debris layer over ice.

3. Research Methodology.

3.1 Data collection and Field work

For this study we conducted three field campaigns, first in October 2024, at the beginning of the ablation season; a second in February 2025; and the last in April 2025, at the end of the season. During each field campaign, multispectral images was taken with a commercial UAV "DJI 3Multiespectral", equipped with a GNSS antenna, a 20-megapixel (MP) RGB camera and 5-MP multispectral cameras able to capture images in the

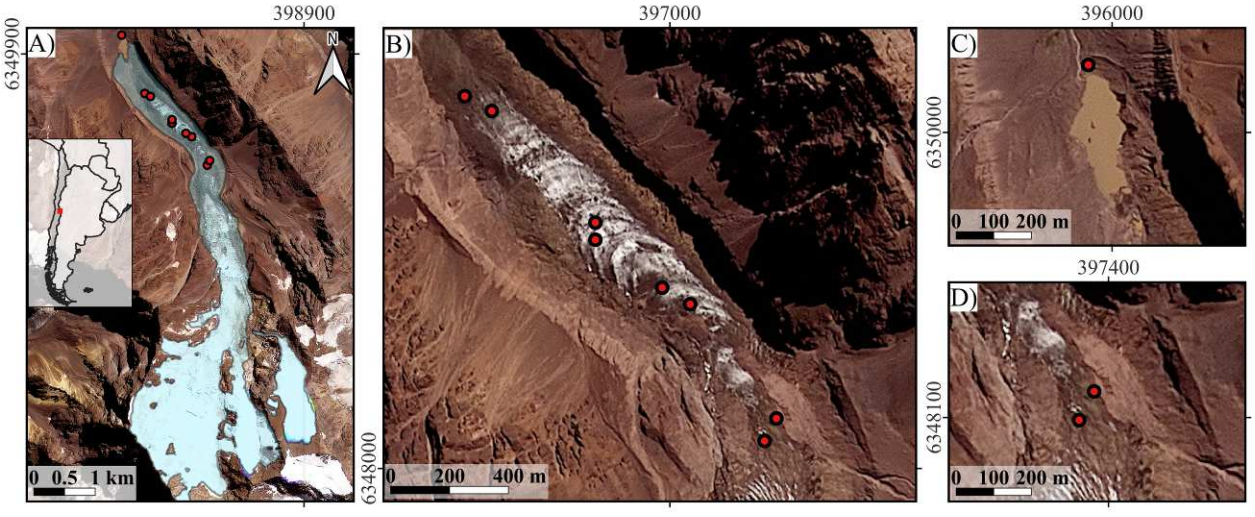

Figure 1: Study area. A) Glacier location. B) sampling distribution. C) frontal moraine control location. D) upper debris site collection and debris flow.

This contribution has been peer-reviewed. The double-blind peer-review was conducted on the basis of the full paper.
https://doi.org/10.5194/isprs-annals-X-3-W4-2025-263-2026 | © Author(s) 2026. CC BY 4.0 License.

following bands: green (g) 560±16nm, red (r) 650±16nm, red edge (re) 730±16nm and near infrared (nir) 860±26nm. For better georeferencing, an Emlid RS2 GNSS antenna was installed 3 kilometres north of the glacier as a base station.

During February 2025 field campaign, as can be seem in Figure 1B, eight locations were selected for debris thickness and coverage measurements. An additional site was selected as control place at the frontal moraine (figure 1C).

For debris measurements, once the site was selected, we marked an area of $1m^2$ as shown in Figure 2. At each measurement site, we carried out 100 individual thickness measurements and calculated the percentage of debris cover (Table 2).

3.2 UAV and multispectral data processing.

After the UAV flight was completed, each band was individually processed and radiometrically calibrated at the software Pix4D to generate an orthomosaic for each band (Daniels 2023). Once the orthomosaic were created, the images were co-registrated and aligned in Qgis version 3.40 using the Co-Registration plugin, based on the AROSICS method (Scheffler et al. 2017).

To elaborate a spectral index, we adapted and simplified the methodology of Hou et al. 2014 for hyperspectral images to make it suitable for multispectral images. As shows in Figure 3, two shoulders were found in the band g, re and nir, and red band was used as the absorption band with the minimum value.

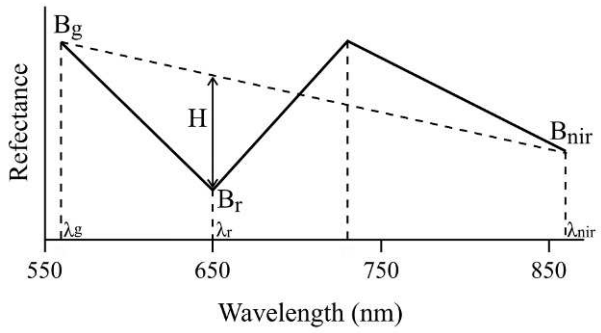

Figure 3: Exaggerated Spectral features and spectral index model.

The spectral index (SI) was created using the raster calculator tool in Qgis software, following the equations below. Equation 1 describes a simple straight-line between shoulders as detailed in Figure 3.

$$B_i = m\lambda_i + c \quad (1)$$

Here, B_i represents the reflectance of any band in the line, m the slope of the line, λ_i represent band wavelength and c is the intercept constant. Equations 2 and 3 are needed to describe the straight-line equation, Equation 2 describes the slope "m" of the line, Equation 3 calculates the constant "c", and Equation 4 expresses the difference H between real B_r value and its point on the projected line as can be seen in figure 3

$$m = \frac{B_{nir} - B_g}{\lambda_{nir} - \lambda_g} \quad (2)$$

$$c = B_{nir} - m\lambda_{nir} \quad (3)$$

$$H = m\lambda_r + c - B_r \quad (4)$$

$$SI = Hm\ ; \begin{cases} SI > 0.015 & \text{Exposed ice} \\ -0.0035 < SI < 0.015 & \text{Transition zone} \\ SI < -0.0035 & \text{Debris cover} \end{cases} \quad (5)$$

In these equations, B_{nir}, B_g and B_r represent the intensity of bands nir and Green and red respectively; (m) and (c) are the slope and intercept of the line between B_{nir} and B_g and λ_{nir}, λ_g and λ_r corresponds to the wavelengths of its respective bands. H is the distance between the B_r value and its point on the calculated line.

Finally, Equation 5 describes the resulting spectral index, obtained by multiplying Equations 2 and 4. The raster resulting from this spectral index was then used to perform a supervised classification to determine the thresholds distinguishing debris-covered areas, exposed ice, and transition zones. Subsequently, Equation 6 was applied to separate the raster into three distinct polygons, each representing one of these surface types along with their corresponding areas.

4. Results.

The results of the study are presented below. Table 1 shows coordinates of each sampling and control point. While table 2 report debris cover thickness measure during field work, in general debris cover zones have at least a 4cm thick layer of debris (figure 2A), transition zones have up to 1.5 cm thick layer of debris and some big and disperse rocks intercalated with small, uncovered ice patches (figure 2B). Ice zones show some disperse clasts, rocks and it is common to find patches of debris with a few millimetres thick (figure 2C).

Id	Sample name	UTM East	UTM North
01	DGJN01	397322	6348093
02	DGJN02	397362	6348169
03	DGJN03	396303	6349260
04	DGJN04	396395	6349210
05	DGJN05	395927	6350206
06	DGJN06	397069	6348556
07	DGJN07	396974	6348612
08	DGJN08	396747	6348774
09	DGJN09	396747	6348832

Table 1: Sampling points

Id	Sample name	Debris thickness (cm)	Classification
01	DGJN01	4	Debris cover
02	DGJN02	49	Debris cover
03	DGJN03	1.3	Transition zone
04	DGJN04	0.9	Transition zone
05	DGJN05	-	Moraine
06	DGJN06	0.1	Exposed Ice
07	DGJN07	1.1	Transition zone
08	DGJN08	0	Exposed Ice
09	DGJN09	0.3	Transition zone

Table 2: Debris cover thickness and fieldwork classification.

Figure 4 displays the results of the direct observation of the multispectral cameras for each control and measurement point on the glacier tongue. For exposed ice, slopes between the bands green and nir are shallower and negative, H value are larger, and reflexion intensity is usually higher. Debris covered areas show positive slopes and smaller or negative H values. Between the two, transition zones are characterized for thin debris layers and dispersed patches of exposed ice, typically exhibiting very shallow or nearly flat slopes.

After the image preparation described in section 3.2 and based on the spectral feature described above we created a spectral index (SI) by multiplying the slope by the H value, as can be seen in Equation 5, this amplifies the numerical difference between debris cover areas, transition zones and exposed ice, allowing them to be classified based by the resulting value.

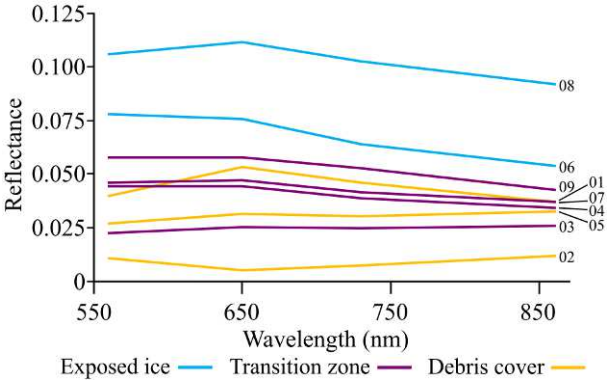

Figure 4: Spectral response and field classification**.**

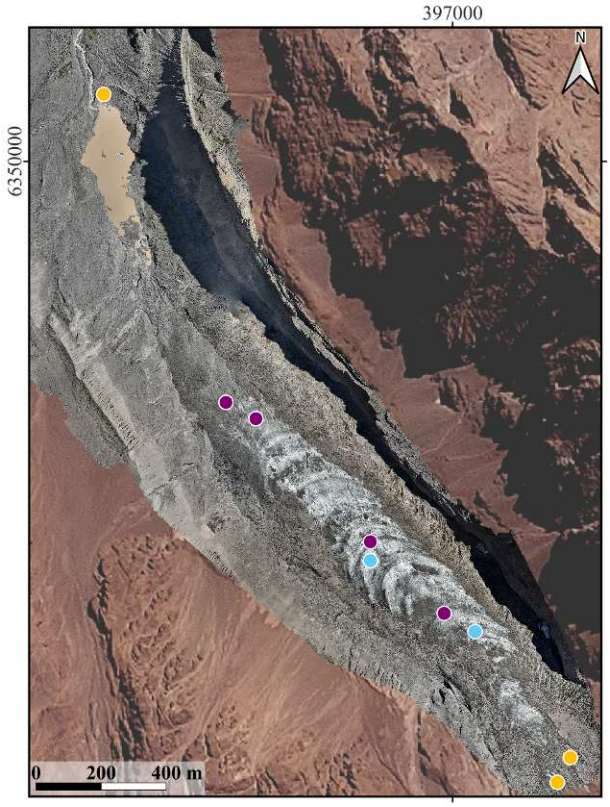

Figure 6: RGB orthomosaic with the sampling points classified on basis of table 2.

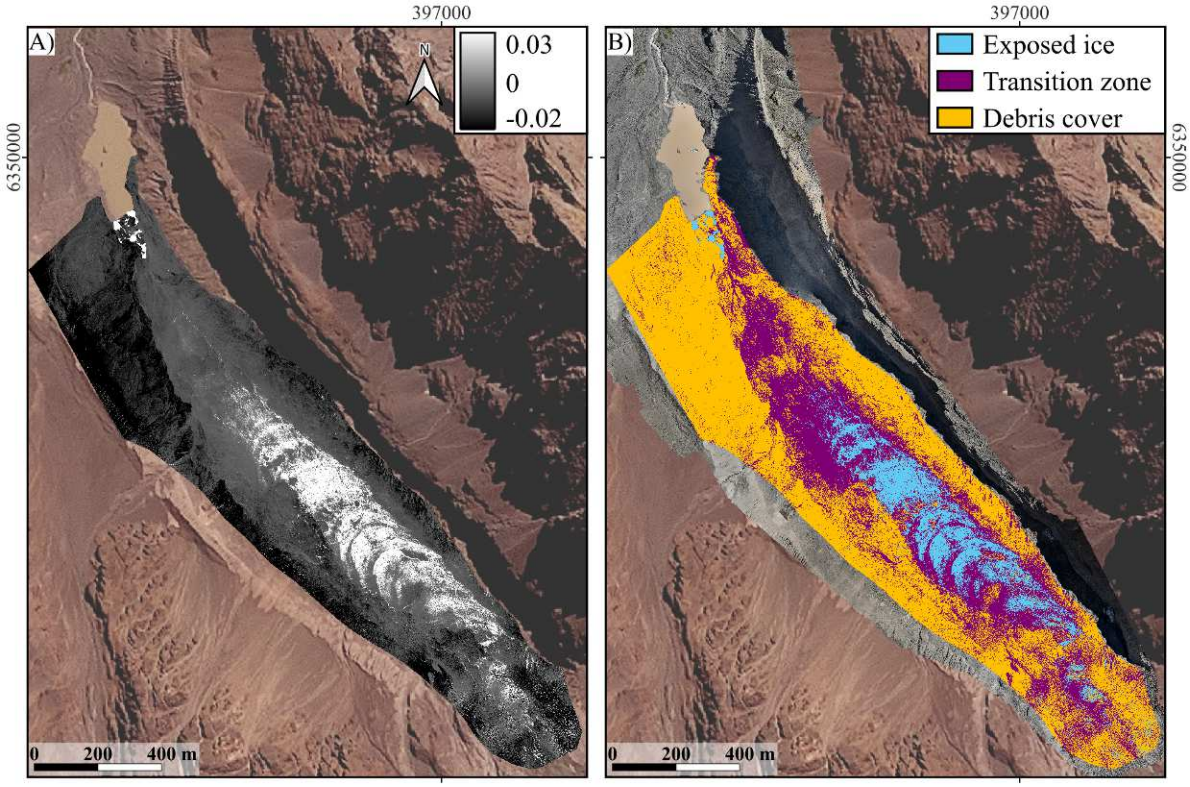

Figure 5: Spectral index and Orthomosaic results. A) SI results in a continuum grey scale. B) SI classification based on Equation 5 discrete intervals.

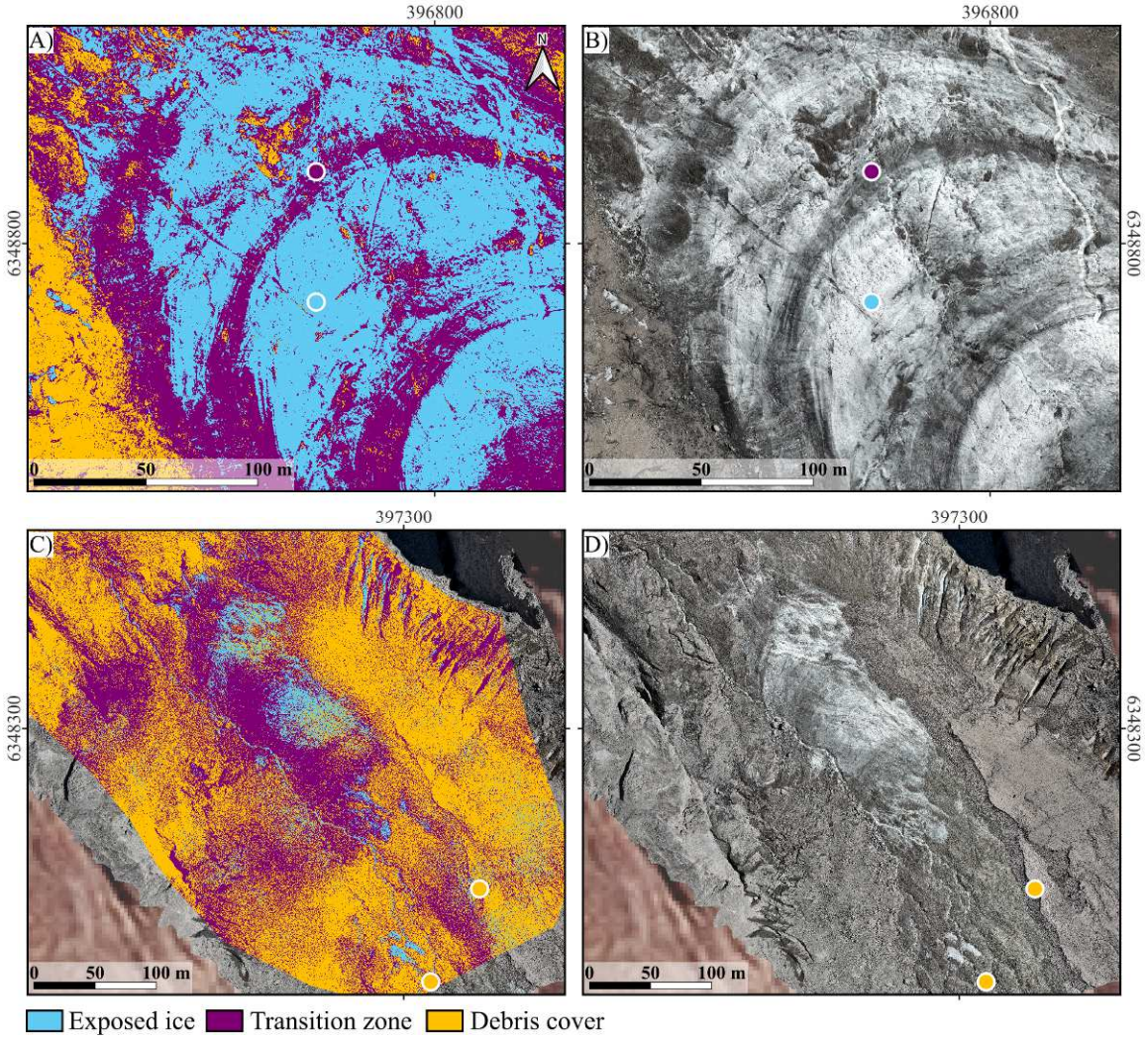

Figure 7: Detail map of SI model. A) SI model for central tongue. B) RGB imagery from central tongue. C) SI model for the upper part of the tongue. D) RGB map for the upper part of the tongue.

Figure 6 provides an overview of the ablation tongue featuring An RGB orthomosaic with the field debris measurements and classification points on based on thickness and debris density observed on field work.

The Spectral Index (SI) is shown in Figure 5A, with negative values corresponding to debris-covered glacier areas, positive values corresponding to exposed ice, and values closer to zero representing transition zones. Figure 5B shows the results of the supervised classification based on the SI. Using this classification, the discrete intervals in Equation 5 were defined. The outcome of the classification of the full ablation tongue is presented in Figure 5 B, highlighting the spatial distribution of debris and clearly illustrating the bare ice areas. This can be compared with Figure 5A, which shows the raw SI values.

5. Discussion.

Field control points were collected at eight locations across the ablation tongue, providing a good overview of the variability in debris cover. The selected points include two sites on glacier ice with thick supraglacial debris, two on exposed ice, and four within the transitional zone. This spatial distribution offers balanced coverage of the different surface conditions present in the study area, as illustrated in Figure 6. These field observations align well with the debris patterns identified by the modeled Spectral Index (SI) shown in Figure 7, supporting the reliability of the classification approach. Of the four spectral bands analyzed—green, red, red edge (RE), and near-infrared (NIR)—the green and NIR bands were selected to compute the slope used in the spectral index. Among the full set, the RE band did not show a good and consistent variation between areas with thick and thin debris cover, limiting its usefulness for debris thickness differentiation. In contrast, the NIR band demonstrated a more pronounced sensitivity to both exposed ice and changes in debris thickness, making it particularly valuable for distinguishing surface conditions and supporting the construction of the index. In general, reflectance and patterns are similar to those reported by Jawak et al. (2022), considering that the flights were carried out before sunrise over the mountains, which resulted in lower overall intensity.

The debris thickness maps derived from the spectral index provide a detailed visualization of spatial heterogeneity across the glacier's ablation zone. Figure 5B highlights exposed ice zones with notable clarity, particularly along the central axis of the ablation tongue, as seen in the corresponding RGB image (Figure 6). The spectral index also effectively delineates the heavily debris-covered area in the northeastern sector of the

glacier tongue—a zone that is too hazardous to access on foot—demonstrating the value of remote sensing in otherwise inaccessible terrain. Additionally, the index reliably identifies transitional debris zones near the centre of the tongue and, most notably, at the glacier front southeast of the proglacial lake. In this latter sector, the spectral response indicates a transition zone with scattered ice patches, which is consistent with field observations reporting a debris thickness of less than one centimetre. This area is characterized by the presence of supraglacial streams and crevasses—features that are not easily distinguished in the RGB imagery of Figure 6 but were confirmed during field visits. These examples illustrate the potential of the index to resolve subtle debris variations that are difficult to detect using conventional imagery alone.

Building on the patterns observed in Figure 5, Figure 7A and 7B offer a more detailed view of the central ablation tongue. The index in Figure 7A clearly delineates exposed ice and identifies a series of transverse debris bands interpreted as arcuate structures that surround step-like features resembling glacier ogives. These features are also visible in the RGB orthomosaic (Figure 7B) and are located on the steepest slope section of the ogive system. The debris bands consist of a thin, discontinuous layer of scattered clasts only a few millimeters thick. Further upslope, Figures 7C and 7D show the upper portion of the tongue, where the model primarily identifies debris-covered glacier surface, with a central zone of exposed ice and alternating thick and thin debris layers to the southwest. Notably, in the northeastern fringe, the index captures a large debris-covered area corresponding to a debris flow event that occurred in January 2024, which deposited material up to 50 cm thick—serving as a valuable control point for index interpretation. Just north of this deposit, the model also highlights steep ice cliffs formed within the debris-covered glacier, which are identifiable in both the spectral and RGB imagery.

Despite the overall consistency of the index results, several limitations are evident in specific areas of the model. In the northwestern sector, a steep lateral slope interpreted as a lateral moraine in the RGB imagery contains visible ice exposures in small landslides and ice cliffs. In this zone, the spectral index loses reliability, introducing artifacts that incorrectly classify parts of the surface as thin debris cover. Similar inconsistencies are found at the margins of the model, where very steep slopes and deep shadows reduce the quality of the orthomosaic, especially near exposed ice outcrops and in areas with poor radiometric contrast. These shadowed regions were excluded from the final index classification due to low data quality. A comparable issue affects the proglacial lake, which was also excluded from the model because of spectral confusion and geometric distortions in the orthomosaic generation. These examples highlight the influence of terrain geometry and illumination conditions on the robustness of the method, especially in complex or heterogeneous surface types.

Future work will focus on strengthening the classification through statistical validation using satellite-derived datasets and comparison with existing geodetic mass balance estimates. Additional UAV flights under varying illumination conditions and at different times of the season are also planned to assess the temporal consistency and sensitivity of the spectral index.

6. Conclusion.

This study demonstrates the potential of a simple spectral index derived from UAV multispectral imagery to qualitatively classify glacier debris thickness and distribution in a remote high-mountain environment. The index effectively distinguishes exposed ice, debris-covered zones, and transitional areas across the ablation tongue, aligning well with field observations, including regions that are otherwise inaccessible. While the method presents limitations in shadowed or steep terrain, the results offer a valuable descriptive tool for glacier surface characterization. Ongoing work will focus on refining the classification through statistical validation, integration with satellite data, and comparison with geodetic mass balance records, aiming to improve its applicability for long-term glacier monitoring.

7. Acknowledgements

We would like to express our sincere thanks to Parque Andino Juncal for their support over the past five years of field campaigns and flights. We also wish to thank the Laboratorio de Análisis Isotópicos at the Universidad Andrés Bello, and Centro de investigacion GAIA – Antártica at the Universidad de Magallanes for their assistance during the 2024-2025 monitoring campaign. Special thanks go to the field team for their invaluable help with debris measurements and UAV operations.

8. References

Blöthe, J. H., Halla, C., Schwalbe, E., Bottegal, E., Trombotto Liaudat, D., & Schrott, L. (2021). Surface velocity fields of active rock glaciers and ice-debris complexes in the Central Andes of Argentina. *Earth Surface Processes and Landforms*, *46*, 504-522. https://doi.org/DOI: 10.1002/esp.5042.

Daniels, L., Eeckhout, E., Wieme, J., Dejaegher, Y., audenaert, K., & Maes, W. H. (2023). Identifying the Optimal Radiometric Calibration Method for UAV-Based Multispectral Imaging. *Remote Sensing*, *15*(2909). https://doi.org/10.3390/rs15112909

Dorofy, P., Nazari, R., Peter, R., & Key, J. (2016). Development of a Mid-Infrared Sea and Lake Ice Index (MISI) Using the GOES Imager. *Remote Sensing*, *8*(1015). https://doi.org/doi:10.3390/rs8121015

Evans, D. (2018). *Till: A Glacial Process Sedimentology* (Primera edición). Wiley Blackwell.

Falaschi, D., Rivera, A., Lo Vecchio Repetto, A., Moragues, S., Villalba, R., Rastner, P., Zeller, J., & Salcedo, A. (2021). Evolution of Surface Characteristics of Three Debris-Covered Glaciers in the Patagonian Andes From 1958 to 2020. Fron. Earth Sci, 9. https://doi.org/doi: 10.3389/feart.2021.671854

Fyffe, C., Woodget, A., Kirkbride, M., Deline, P., Westoby, M., & Brock, B. (2020). Processes at the margins of supraglacial debris cover: Quantifying dirty ice ablation and debris redistribution. *Earth Surface Processes and Landforms*, *45*, 2272-2290. https://doi.org/DOI: 10.1002/esp.4879

Herreid, S., & Pellicciotti, F. (2020). The state of rock debris covering Earth's glaciers. *Nature Geoscience*, *13*, 621-627. https://doi.org/10.1038/s41561-020-0615-0

Huo, D., Bishop, M., & Bush, A. (2021). Understanding Complex Debris-Covered Glaciers: Concepts, Issues, and Research Directions. *Fron. Earth Sci*, *9*. https://doi.org/doi: 10.3389/feart.2021.652279

Huo, H., Ni, Z., Jiang, X., Zhou, P., & Liu, L. (2014). Mineral Mapping and Ore Prospecting with HyMap Data over Eastern Tien Shan, Xinjiang Uyghur Autonomous Region. Remote Sensing, 6, 11829-11851. https://doi.org/doi:10.3390/rs61211829

Jawak, S. D., Wankhede, S. F., Luis, A. J., & Balakrishna, K. (2022). Multispectral Characteristics of Glacier Surface Facies (Chandra-Bhaga Basin, Himalaya, and Ny-Ålesund, Svalbard) through Investigations of Pixel and Object-Based Mapping Using Variable Processing Routines. *Remote Sensing*, *14*(6311). https://doi.org/%2010.3390/rs14246311

Jones, D. B., Harrison, S., & Anderson, K. (2019). Mountain glacier-to-rock glacier transition. *Global and Planetary Change*, *181*. https://doi.org/10.1016/j.gloplacha.2019.102999

Kirkbride, M., & Deline, P. (2013). The formation of supraglacial debris covers by primary dispersal from transverse englacial debris bands. *Earth Surface Processes and Landforms*, *38*, 1779-1792. https://doi.org/DOI: 10.1002/esp.3416

Lukas, S., Benn, D., Boston, C., Brook, M., Coray, S., Evans, D., Graf, A., Keller-Pirklbauer, A., Kirkbride, M., Krabbendam, M., Lovell, H., Machiedo, M., Mills, S., Nye, K., Reinardy, B., Ross, F., & Signer, M. (2013). Clast shape analysis and clast transport paths in glacial environments: A critical review of methods and the role of lithology. *Earth-Science Reviews*, *121*, 96-116. http://dx.doi.org/10.1016/j.earscirev.2013.02.005

Monnier, S., & Kinnard, C. (2015). Reconsidering the glacier to rock glacier transformation problem: New insights from the central Andes of Chile. *Geomorphology*, *238*, 47-55. http://dx.doi.org/10.1016/j.geomorph.2015.02.025

Nicholson, L., & Benn, D. (2013). Properties of natural supraglacial debris in relation to modelling sub-debris ice ablation. *Earth Surface Processes*, *38*, 490-501. https://doi.org/DOI: 10.1002/esp.3299

Östrem, G. (1959). Ice Melting under a Thin Layer of Moraine, and the Existence of Ice Cores in Moraine Ridges. *Geografiska Annaler*, *41*(4), 228-230.

Pellicciotti, F., Ragettli, S., Carenzo, M., & McPhee, J. (2013). Changes of glaciers in the Andes of Chile and priorities for future work. *Science of the Total Environment*, *493*, 1197-1210. http://dx.doi.org/10.1016/j.scitotenv.2013.10.055

Racoviteanu, A. E., Williams, M. W., & Barry, R. G. (2008). Optical Remote Sensing of Glacier Characteristics: A Review with Focus on the Himalaya. *Sensors*, *8*, 3355-3383. https://doi.org/DOI:%252010.3390/s8053355

Rounce, D. R., Hock, R., McNabb, R. W., Millan, R., Sommer, C., Braun, M. H., Malz, P., Maussion, F., Mouginot, J., Seehaus, T. C., & Shean, D. E. (2021). Distributed Global Debris Thickness Estimates Reveal Debris Significantly Impacts Glacier Mass Balance. *Geophysical research letters*, *48*. https://doi. org/10.1029/2020GL091311

Sato, Y., Fujita, K., Inoue, H., Sunako, S., Sakai, A., Tsushima, A., Podolskiy, E., Kayastha, R., & Kayastha, R. B. (2021). Ice Cliff Dynamics of Debris-Covered Trakarding Glacier in the Rolwaling Region, Nepal Himalaya. *Fron. Earth Sci*, *9*. https://doi.org/doi: 10.3389/feart.2021.623623

Scheffler, D., Hollstein, A., Diedrich, H., Segl, K., & Hostert, P. (2017). AROSICS: An Automated and Robust Open-Source Image Co-Registration Software for Multi-Sensor Satellite Data. Remote Sensing, 9(676). https://doi.org/doi:10.3390/rs9070676

van Woerkom, T., Steiner, J., Kraaijenbrink, P., Miles, E., & Immerzeel, W. (2019). Sediment supply from lateral moraines to a debris-covered glacier in the Himalaya. *Earth Surf. Dynam.*, *7*, 411-427. https://doi.org/10.5194/esurf-7-411-2019